

**The *C. elegans* Dosage Compensation Machinery Is Recruited to
X-Chromosome DNA Attached to an Autosome**

**Jason D. Lieb^{1,4}, Carlos Ortiz de Solorzano², Enrique Garcia Rodriguez², Arthur Jones²,
Michael Angelo³, Stephen Lockett², and Barbara J. Meyer¹**

¹Howard Hughes Medical Institute and University of California, Berkeley

²Lawrence Berkeley National Laboratory

³Whitehead Institute and Massachusetts Institute of Technology

Corresponding author: Dr. Barbara J. Meyer,
HHMI and Department of Molecular and Cell Biology,
University of California, Berkeley, CA 94720-3204.
E-mail: bjmeyer@uclink4.berkeley.edu

⁴ Present address: HHMI and Stanford University Medical Center,
Department of Biochemistry, B439 Beckman Center, Stanford, CA 94305-5428

Running header: X-chromosome Recognition in *C. elegans*

Individual responsible for examining proofs, ordering reprints, and arranging for the payment of
page charges:

Dr. Barbara J. Meyer

Howard Hughes Medical Institute

Department of Molecular and Cell Biology

401 Barker Hall #3204

University of California

Berkeley, CA 94720-3204

E-mail: bjmeyer@uclink4.berkeley.edu

FAX: (510) 643-5584

Phone: (510) 643-5585

ABSTRACT

The dosage compensation machinery of *C. elegans* is targeted specifically to the *X* chromosomes of hermaphrodites (*XX*) to reduce gene expression by half. Many of the *trans*-acting factors that direct the dosage compensation machinery to *X* have been identified, but none of the proposed *cis*-acting *X*-chromosome-recognition elements needed to recruit dosage compensation components have been found. To study *X*-chromosome recognition, we explored whether portions of an *X* chromosome attached to an autosome are competent to bind the *C. elegans* dosage compensation complex (DCC). To do so, we devised a three-dimensional *in situ* approach that allowed us to compare the volume, position and number of chromosomal and sub-chromosomal bodies bound by the dosage compensation machinery in wild-type *XX* nuclei and *XX* nuclei carrying an *X* duplication. The dosage compensation complex was found to associate with a duplication of the right 30% of *X*, but the complex did not spread onto adjacent autosomal sequences. This result indicates that all the information required to specify *X*-chromosome identity resides on the duplication and that the dosage compensation machinery can localize to a site distinct from the full-length hermaphrodite *X* chromosome. In contrast, smaller duplications of other regions of *X* appeared not to support localization of the DCC. In a separate effort to identify *cis*-acting *X*-recognition elements, we used a computational approach to analyze genomic DNA sequences for the presence of short motifs that were abundant and over-represented on *X* relative to autosomes. Fourteen families of *X*-enriched motifs were discovered and mapped onto the *X* chromosome.

INTRODUCTION

Dosage compensation is an essential, chromosome-wide regulatory process that equalizes expression of most *X*-linked genes between males (usually *XO* or *XY*) and females (usually *XX*), despite their two-fold difference in *X*-chromosome dose. Flies, worms, and mammals utilize diverse mechanisms of dosage compensation, but all involve global changes in *X*-chromosome structure that ultimately serve to adjust the level of *X*-linked transcripts in only one sex (CLINE and MEYER 1996; MELLER 2000; MEYER 2000). These *X*-chromosome changes are mediated by dosage compensation machinery that must recognize and associate specifically with the *X* chromosome(s) of only the dosage-compensating sex. Although the identity and properties of proteins and non-coding RNAs that execute dosage compensation is known in detail, much less is known about the *cis*-acting factors that must reside on the *X* chromosome to recruit the dosage compensation machinery. Important advances in understanding the problem of *X*-chromosome recognition have come from analysis of dosage compensation in mammals and *Drosophila melanogaster*.

Female placental mammals (*XX*) inactivate one of their two *X* chromosomes to achieve levels of *X*-chromosome expression equal to those of the *XY* male (LEE and JAENISCH 1997). The inactivated mammalian *X* chromosome is hypo-acetylated, hyper-methylated and hyper-condensed to form a structure called the Barr body (JEPPSEN and TURNER 1993; LYON 1961; MOHANDAS *et al.* 1981). *X* inactivation is initiated at a small *cis*-acting locus on the *X* chromosome, the *X* Inactivation Center (*Xic*) (HERZING *et al.* 1997; LEE *et al.* 1999; LEE *et al.* 1996), which has been localized to an 80 kb fragment that can confer inactivation properties onto autosomes (LEE *et al.* 1999). Encoded within the *Xic* is a non-coding RNA called *Xist*, which helps choose the specific *X* chromosome(s) to be inactivated (MARAHRENS *et al.* 1998), and then

spreads in *cis* along the future inactive *X* (CLEMSON *et al.* 1996; PENNY *et al.* 1996). Although *Xist* is not required for the maintenance of the inactive state (CSANKOVSKI *et al.* 1999), it may function to recruit specialized repressive chromatin components to *X* at the onset of inactivation (BROWN and WILLARD 1994; LEE and JAENISCH 1997). Regulation of *Xist* and hence *X* inactivation is achieved in part by a non-coding 40 kb transcript called *Tsix* that is antisense to and spans the *Xist* gene. A female *X* chromosome that cannot transcribe *Tsix* is destined to be inactivated, suggesting that *Tsix* is involved in *X*-chromosome choice and negatively regulates *Xist* (LEE and LU 1999). Together these studies indicate that the *Xist* locus serves as the primary *cis*-acting element in *X*-chromosome recognition, and that the dosage compensation machinery associates with *X* by a nucleation and spreading mechanism. Furthermore, no broadly distributed *X*-specific sequences are required for *Xist* binding or propagation.

In contrast to mammals, *Drosophila* males (*XY*) compensate for their lower *X*-chromosome dose by hyper-transcribing their single *X*. Dosage compensation is implemented by the male-specific lethal genes *msl1*, *msl2*, *msl3*, *mle*, and *mof* whose products form a complex that associates specifically with hundreds of sites along the male *X* chromosome (BASHAW and BAKER 1995; GORMAN *et al.* 1995; GORMAN *et al.* 1993; KELLEY *et al.* 1995; KURODA *et al.* 1991; PALMER *et al.* 1993; ZHOU *et al.* 1995). In flies mutant for an *msl* gene, partial MSL complexes localize to a subset (30-40) of sites along the *X* (GORMAN *et al.* 1995; GU *et al.* 1998; LYMAN *et al.* 1997; PALMER *et al.* 1994). In a surprising parallel to mammalian dosage compensation, an RNA component was discovered in the *Drosophila* dosage compensation machinery. Two untranslated RNAs, *roX1* and *roX2*, co-localize to the male *X* chromosome in an MSL complex-dependent manner (AMREIN and AXEL 1997; MELLER *et al.* 1997). The *roX1* and *roX2* loci themselves correspond to two of the sites that retain MSL binding in *msl* mutants

(KELLEY *et al.* 1999). Unlike individual *X*-derived genes that fail to retain MSL binding when moved to autosomes (BHADRA *et al.* 1999; BONE and KURODA 1996), the *roX1* gene can recruit MSL proteins to autosomes, and the proteins can then spread onto flanking autosomal genes (KELLEY *et al.* 1999). These results suggest that *roX* genes are *X* chromatin entry sites for the dosage compensation machinery (KELLEY *et al.* 1999). Thus, *Drosophila* appears to use a discrete set of entry sites positioned along the *X* chromosome to recruit the dosage compensation machinery and permit spreading to adjacent genes. The properties of the entry sites that confer the MSL recruitment activity are as yet not understood.

In the nematode *C. elegans*, hermaphrodites (XX) reduce the level of transcripts from each of their two *X* chromosomes by half to equal the expression from the single male *X* (CHUANG *et al.* 1994; MEYER and CASSON 1986; PLENEFISCH *et al.* 1989). Failure to activate dosage compensation in hermaphrodites results in overexpression of *X*-linked genes and lethality (MEYER 1997; NUSBAUM and MEYER 1989; PLENEFISCH *et al.* 1989). *C. elegans* dosage compensation is implemented by a protein complex that localizes specifically to both *X* chromosomes of hermaphrodites at about the 40-cell stage of embryogenesis (Figure 1) (CHUANG *et al.* 1994; CHUANG *et al.* 1996; LIEB *et al.* 1996; LIEB *et al.* 1998). This biochemically and genetically defined dosage compensation complex (DCC) includes proteins specific to dosage compensation (DPY-27) and proteins that also function in chromosome segregation during mitosis (MIX-1) or meiosis (DPY-26 and DPY-28) (CHUANG *et al.* 1994; CHUANG *et al.* 1996; LIEB *et al.* 1996; LIEB *et al.* 1998). DPY-27 and MIX-1 are members of the highly conserved SMC family of proteins, which includes proteins that participate in diverse chromosome behaviors including sister chromatid cohesion, mitotic chromosome condensation and mitotic recombination repair (CHUANG *et al.* 1994; LIEB *et al.* 1998; KOSHLAND AND

STRUNNIKOV 1996). DPY-26 has two small motifs in common with two mitotic proteins: XCAP-H, a component of the *X. laevis* 13S condensin complex (HIRANO *et al.* 1997), and Barren, a *Drosophila* protein essential for mitotic chromosome segregation *in vivo* (BHAT *et al.* 1996). Although DPY-26 is required for the faithful segregation of chromosomes during meiosis (HODGKIN 1983), it has diverged significantly from both homologs and does not appear to function in mitosis (LIEB *et al.* 1996). The X-localization of DPY-26, DPY-27, and MIX-1, and their similarity to proteins involved in chromosome dynamics led to the view that the dosage compensation complex regulates gene expression by altering X-chromosome structure.

Individually, DPY-26, DPY-27, DPY-28 and MIX-1 cannot associate with X, nor can a complex containing all four proteins (CHUANG *et al.* 1996; HSU *et al.* 1995; LIEB *et al.* 1998; LIEB *et al.* 1996). Instead, the hermaphrodite-specific proteins SDC-2 and SDC-3 are required for assembling the complex on X (CHUANG *et al.* 1996; DAVIS and MEYER 1997). SDC-2 activates the dosage compensation process and confers hermaphrodite specificity: its product is present exclusively in XX animals and its ectopic expression in males causes inappropriate dosage compensation and death, unlike any other dosage compensation protein (DAWES *et al.* 1999; NUSBAUM and MEYER 1989). SDC-2 may also direct X-recognition, since it can localize to the X in the absence of the other known DCC components or dosage compensation genes. Several lines of evidence indicate that SDC-2 collaborates with SDC-3 to target the dosage compensation machinery to X. SDC-3 also associates with X, it contains a pair of TFIIIA-type zinc finger motifs that are essential for assembly of the DCC on X, and it acts synergistically with SDC-2 to kill males when overexpressed (DAVIS and MEYER 1997; DAWES *et al.* 1999; DELONG *et al.* 1993; KLEIN and MEYER 1993).

A reasonable hypothesis for *X* recognition is that *cis*-acting DNA elements on the *C. elegans* *X* chromosome allow *trans*-acting factors like the SDC proteins to associate with *X* and thereby recruit the dosage compensation machinery. Such elements have not yet been identified. *X* recognition has been particularly difficult to approach in *C. elegans* because of a lack of candidate *X*-recognition elements, the inability to make directed chromosomal insertions or deletions, and the extremely small size of somatic chromosomes. In this study, two general strategies were pursued in an attempt to overcome these obstacles and to identify *cis*-acting *X*-recognition elements. The first was to determine whether portions of the *X* chromosome attached to an autosome are competent to bind the dosage compensation complex, and if so whether this binding spreads into the autosomal region. This was accomplished with a novel three-dimensional *in situ* approach that allowed us to compare the volume, position, and number of DCC foci between wild-type nuclei and nuclei homozygous for autosome-attached duplications of different portions of *X*. The second strategy utilized a computational approach to identify *X*-chromosome-enriched sequence motifs.

MATERIALS AND METHODS

Strains: Animals were maintained on NG agar plates with *Escherichia coli* OP50 as a food source (BRENNER 1974). The following strains were used in this study:

TY0125	wild type (N2)
SP0117	<i>mnDp10(X;I); unc-3(e151) X</i>
TY2025	<i>yDp14(X;I); unc-2(e55) X</i>
SP0076	<i>mnDp27(X;II); unc-3(e151) X</i>
TY0689	<i>stDp2(X;II); dpy-6(e14) X</i>

Antibody staining: For each experiment, wild-type and duplication-bearing embryos were prepared in parallel using identical reagents, and the samples were subjected to confocal microscopy on the same day. 10-30 gravid adult worms were transferred to a positively charged glass slide (Permafroast Plus, Fisher) in 6 μ l of M9 buffer. An incision was made at the vulva to release the embryos. An 18 x 18 mm cover slip was placed on top of the sample, and the slide was placed directly on a block of dry ice for at least 10 min. The cover slip was then removed from the slide with a quick downward stroke of a single-edged razor. The slide was immediately placed in 95% ethanol for 1 min, and then incubated in PBS for 5 min. Most of the PBS was wicked away, and 50 μ l of fixative (4% paraformaldehyde, 18% methanol, 3 mM EGTA, 64 mM KCl, 16 mM NaCl, 0.4 mM spermidine-HCl, 0.16 mM spermine, 0.4 % β -mercaptoethanol, 12 mM PIPES (pH 7.4)) was placed directly on the sample and covered with a 30 X 30 mm piece of parafilm. The slides were then placed on ice for 20-30 min. The fixative was removed from the samples by placing the slide into a vessel containing PBS (15 min), and washed 15 min in PBSTB (1 x PBS, 0.1% BSA, 0.5% Tween 20, 0.05% Azide, 1 mM EDTA), and 15 min PBSTA (1 x PBS, 1% BSA, 0.5% Tween 20, 0.05% Sodium azide, 1 mM EDTA). A 30 μ l dilution of the primary antibody in PBSTA (1:100) was then placed on the sample, which was covered with a 30 X 30 mm piece of parafilm. The slide was placed in a humidified chamber for 4 hr at room temperature. The slides were washed as before and the secondary antibody was applied in the same manner as the primary. After washing as before, 200 μ g/mL RNase was then placed on samples, which were incubated at 37 °C for 1 hr. The samples were washed and incubated with 2 μ g/mL propidium iodide for 1 hr, washed, and mounted for confocal microscopy. An N-propyl gallate/glycerol mix (2% n-propyl galate, 30 mM Tris-HCl pH 9.5, 70% glycerol) mix was used as an anti-fade reagent in the mount.

Detection of extrachromosomal arrays: Wild-type worms were transformed with pRF4, a plasmid encoding *rol-6(su1006)* (a marker for transgenic worms), pSV2-dhFr8.32 a plasmid containing 32 copies of tandem *lacO* repeats (CARMI *et al.* 1998; DAWES *et al.* 1999; STRAIGHT *et al.* 1996), and pPD49-78, which expresses LACI-GFP under control of the *hsp-16* heat shock promoter (Gonzalez-Serricchio, A and Sternberg, P., personal communication). Worms were raised at 20°C, heat shocked for 30 min at 37°C to express LACI-GFP, and allowed to recover for 30 min at 20°C. The LACI-GFP binds to the *lac* operator sequences in the array, allowing the extrachromosomal arrays to be detected by antibodies to GFP. The worms were then prepared for microscopy as described above except their DNA was stained with 50 µg/ml of diamidinophenolindole (DAPI) included in DABCO/glycerol mount at neutral pH.

Microscopy: For experiments using duplications, microscopy was carried out on a Zeiss 410 confocal microscope (Experiments 1 and 2) or a Leica TCS NT confocal (Experiments 3, and 4). For array experiments, microscopy was performed on the Leica confocal microscope. All images were acquired with a 63X oil-immersion objective (NA= 1.32) at a zoom of 3 with a 512 X 512 image size, pinhole =1. Photomultiplier settings were determined automatically by the computer (Zeiss) or determined manually using the “glow over” look-up table (Leica). For the Leica, PMT settings were adjusted to maximize signal intensity but minimize saturated pixels. The gain/offset was not adjusted from the default values (a black background was produced). Individual sections were averaged 4 times in “Frame” mode. The step size in the z direction was 300 nm (Zeiss) or 283 nm (Leica), creating voxels of X=102 nm, Y=102 nm, Z= 300 or 283 nm. At an excitation wavelength of 488 nm (for FITC), the microscopes used in this study have a maximum theoretical xy resolution of approximately 225 nm, and a maximum theoretical z resolution of approximately 280 nm (using a ~140 nm z-step size). In these

experiments, a z-step size of 300 nm was used as a compromise between optimal resolution in z, photo-bleaching effects, and image file size. A 300 nm step size translates into about 60 raw data slices per embryo, and between three and four raw data slices per nucleus.

Image Analysis: Following raw data collection using the software provided by the confocal microscope manufacturer, data stacks were converted to ICS file format (DEAN *et al.* 1990). Custom SCIL-image modules were then used to filter the image stacks, automatically segment the nuclei (MALPICA *et al.* 1997; ORTIZ DE SOLORZANO *et al.* 1999), and automatically segment the DPY staining into discrete 3D bodies (ORTIZ DE SOLORZANO *et al.* 1998). A full description of the filters and settings that were used to process the images is available at <http://www.genetics.org>. Detailed information about using and obtaining SCIL-image is available at: <http://www.tpd.tno.nl/TPD/smartsite64.html>.

After initial segmentation was complete, images were rendered with daVinci (Data Visualization aNd Computer Interaction) (ORTIZ DE SOLORZANO *et al.* 1999). Rendered objects were then scored manually as clusters of multiple nuclei, an individual nucleus, or debris. Rare nuclei that had been inappropriately segmented were re-joined. Objects scored as clusters of nuclei were sent back to SCIL-image and automatically segmented into individual nuclei using a routine based on morphological transformation (Distance Transform) and the watershed algorithm (ORTIZ DE SOLORZANO *et al.* 1999). Objects scored as debris were not considered for further analysis.

For all data sets, objects with a rendered volume of less than $35 \times 10^6 \text{ nm}^3$ were deleted and were not counted in any aspect of the analysis. This cutoff was determined by empirical comparisons of noise in the original confocal data with rendered data, and by considering the optical limit of resolution (an object $300 \text{ nm} \times 300 \text{ nm} \times 300 \text{ nm} = 27 \times 10^6 \text{ nm}^3$). The settings

for the filters used to render the nuclei and chromosomes were chosen conservatively so that only relatively bright signals with sharp edges would be rendered and counted as objects. For a complete description of how the embryos were analyzed, please refer to the supplemental web site at <http://www.genetics.org>.

Sequence Analysis: All programs used for sequence analysis and instructions for their use are available at <http://www.genetics.org>.

Injections of X-Enriched Oligo Pairs: The following oligonucleotide pairs were annealed to form double-stranded DNA, and co-injected into worms along with the DNA components of the *lacI/lacO* system. The resulting extrachromosomal arrays were then assayed for DCC binding activity by staining with antibodies to DCC proteins. The information in parentheses refers to how many repeating units are represented by the oligo:

Clustered Repeats:

1. Left End

Rpt1 (single unit)

JDL117 GTTTTGGTCGCTGCTAATTTTTGGTCATTGCTAATTTTGTAGTCAGTGCTAA

JDL118 TTAGCACTGACTAAAAATTAGCAATGACCAAAAATTAGCAGCGACCAAAAC

Rpt2 (single unit)

JDL119 GGTCAGTGCAACTTAAATTGGTCAGTGCAACTGCAACT

JDL120 AGTTGCAGTTGCACTGACCAATTTAAGTTGCACTGACC

Rpt3 (single unit)

JDL121 GGTC CGTG CACATG TTTTTTGGTCAGTG CACGTGGTTTCTTTTCTTT

JDL122 AAAGAAAAAGAAACCACGTGCACTGACCAAAAAACATGTGCACGGACC

Rpt4 (tandem units)

JDL123 CAGTGCCTATGAAAGATTGGTCAGTGCCTATGAAAGATTGGT

JDL124 ACCAATCTTTCATAGGCACTGACCAATCTTTCATAGGCACTG

2. CeRep27 (not tested)

3. C07D8 (single unit)

JDL111 CCGGCGCCCATTTAAGGGTAAGGAATCGCTCTAAGCGAAA

JDL112 TTTCGCTTAGAGCGATTCCCTTACCCTTAAATGGGCGCCGG

4. Right Center (single unit)

JDL115 AAAACCGCTCCAAAACCGTTCCAATACCGCTCC

JDL116 GGAGCGGTATTGGAACGGTTTTGGAGCGGTTTT

5. Short Clusters (tandem units)

JDL125 CGACCTAGGTCGCTAGGTCGCAGGTCGCAAAGCGACCTAGGTCGCTAGGT–
CGCAGGTCGCAAAG

JDL126 CTTTGCGACCTGCGACCTAGCGACCTAGGTCGCTTTGCGACCTGCGACCT–
AGCGACCTAGGTCG

6. Right End (single unit)

JDL113 GAAGTGCTTTCTGTCTACTCGAAGCAGTGCTGGTGGATGGAGTC

JDL114 GACTCCATCCACCAGCACTGCTTCGAGTACGACAGAAAGCACTTC

Unclustered Repeats:

Unclustered #1(tandem units)

JDL133 AGGCAGTAACGGTTAGGCAGTAACGGTTAGGCAGTAACGGTT

JDL134 AACCGTTACTGCCTAACCGTTACTGCCTAACCGTTACTGCCT

Unclustered #2 (tandem units)

JDL129 AGGTCACGAGAGGTCACGAGAGGTCACGAG

JDL130 CTCGTGACCTCTCGTGACCTCTCGTGACCT

Unclustered #3 (tandem units)

JDL127 AGTCGGTAGTAGTCGGTAGTAGTCGGTAGT

JDL128 ACTACCGACTACTACCGACTACTACCGACT

Unclustered #4 (tandem units)

JDL131 MGGTCAGTGCGMGGTCAGTGCGMGGTCAGTGCG

JDL132 CGCACTGACCKCGCACTGACCKCGCACTGACCK

Unclustered #5 (tandem units)

JDL137 ACTACGTAAACTACGTAAACTACGTAA

JDL138 TTACGTAGTTTACGTAGTTTACGTAGT

Unclustered #6 (tandem units)

JDL139 CCAGTCGTGCCAGTCGTGCCAGTCGTG

JDL140 CACGACTGGCACGACTGGCACGACTGG

Unclustered #7 (tandem units)

JDL135 TTGCGACCTTTGCGACCTTTGCGACCT

JDL136 AGGTCGCAAAGGTCGCAAAGGTCGCAA

Raw Data: All data that was used in this manuscript can be found and downloaded in tabular form at <http://www.genetics.org>

RESULTS

3-D reconstructions accurately determine the size and position of nuclei, X chromosomes and sub-chromosome-sized objects: The comparisons made in this study are based on the three-dimensional (3-D) reconstruction of X chromosomes or other bodies within

the nuclei of individual cells that had been identified by staining with antibodies to the dosage compensation proteins DPY-26 or DPY-27 (referred to as DPY staining). Following confocal microscopy of embryos stained with a DPY antibody and the DNA dye propidium iodide (PI), stacks of images were used to create 3-D reconstructions of the whole embryos, which were then computationally segmented into individual nuclei (MATERIALS AND METHODS). This staining and reconstruction procedure allowed us to determine the size and shape of each nucleus, and of all the DPY-staining bodies within each nucleus. In wild-type *XX* embryos, the two *X* chromosomes can be readily visualized following the 3-D reconstruction of the DPY-staining channel (Figure 2A-F). By using quantitative data to compare wild-type strains with strains bearing an *X*-chromosome duplication, we sought to detect DCC binding to *X* chromosome DNA that was attached to an autosome.

Before assaying DCC binding to autosome-attached *X* duplications, it was necessary to establish that our method was able to detect sub-chromosome sized fluorescent signals that were located apart from *X*, and that these signals could be resolved spatially from the *X* chromosomes. We tested our assay by determining if a small, GFP-labeled extrachromosomal array could be detected and resolved from the *X* chromosomes in wild-type embryos (MATERIALS AND METHODS). Extrachromosomal arrays and the *X* chromosomes are expected to occupy mutually exclusive positions in the nucleus. *XX* embryos carrying arrays with *lacO* operator repeats and *gfp*-tagged *lac* repressor genes were fixed and stained with anti-GFP antibody to label arrays, anti-DPY-27 antibody to label the *X* chromosomes, and DAPI to label all DNA. After confocal microscopy (Figure 2G) and reconstruction (Figure 2H-I), the arrays were easily detected. On average, each array occupied 1.79% of the nuclear volume, and had an average volume of $337 \times 10^6 \text{ nm}^3$, about half the volume of a single *X* chromosome (see below). Our ability to resolve the

X chromosomes and the arrays in three dimensional space inside of *C. elegans* nuclei is important because it suggests that DPY staining located apart from *X* could be resolved spatially from the *X* chromosomes. Therefore, if the DCC were bound to a partial *X*-chromosome duplication attached to an autosome, the binding could be detected by our staining and reconstruction procedure.

Properties of wild-type nuclei and *X* chromosomes during embryonic development:

We determined the general morphological properties of *X* chromosomes in wild-type embryos to establish a firm baseline for comparison to *X*-duplication-bearing embryos. Although all cells of the embryos used in this analysis contained two *X* chromosomes, two separate DPY-staining bodies were observed in only 31.6% of nuclei, while one staining body was observed in 63.6% of nuclei (Table 1). To examine the reason for the disparity between the known and observed number of *X* chromosomes, nuclei with only one recorded staining body were reviewed manually. In many of these nuclei, two DPY-staining bodies were discernible, but were counted as only one by the computer software because the two bodies were separated by a distance less than our limit of resolution or were connected by a “bridge” of fluorescence (Figure 2J). To confirm that *X*-chromosome proximity interfered with the quantitation, comparison was made between total *X*-chromosome volume in nuclei recorded as containing one DPY-staining body (referred to as a “joined” *X*) and the volume each of the DPY-staining bodies in nuclei recorded as having two *X*s (referred to as a “disjoined” *X*). If the joined *X* chromosomes truly represent two *X*s, then the volume of joined bodies should be approximately twice that of each of the individual disjoined bodies. If the joined class of staining bodies represents only one *X*, then the volumes of the two classes should be roughly equal. We found that the average volume of a DPY-staining body in nuclei with one object is $1338 \times 10^6 \text{ nm}^3$ ($\pm 18 \times 10^6$, standard error), and

in nuclei with two objects is $678 \times 10^6 \text{ nm}^3$ ($\pm 17 \times 10^6$, standard error, Figure 3A). These results indicate that nuclei recorded as having one object actually contain two *X* chromosomes, as expected. This conclusion is confirmed by the observation that DPY staining occupies a similar total volume in nuclei that contain one staining body as in nuclei that contain two staining bodies (Figure 3B). The failure to resolve the two *X* chromosomes in nearly two-thirds of wild-type nuclei is important to consider when interpreting results from duplication strains.

Another expectation is that more than two bodies of DPY staining should never be visible in the nuclei of wild-type embryos. However, in wild-type nuclei, three bodies of staining were observed 4.2% of the time, and four bodies in 0.5% of nuclei. These rare nuclei may contain an *X* chromosome with a weakly staining region that causes it to be counted as two separate bodies, or a spurious antibody signal that creates an artifactual object. Possibly, a small fraction of nuclei were captured in early anaphase of mitosis and therefore do contain more than two discernable *X* chromosomes.

Finally, it was essential to ensure that our analysis was not skewed by differences in nuclear or chromosomal architecture that may occur throughout embryonic development. Therefore, we determined how nuclear volume and *X*-chromosome volume varied with each other, and how they varied with embryonic age. We expected that nuclear volume, as determined by PI staining, would decrease as the embryos aged because the size of the chitinous egg shell remains constant throughout embryonic development, while the embryo's cell number increases from one to 558. As expected, we observed that the average nuclear volume decreases as embryos develop (Figure 4A, age range 26 to 368 cells). One might also expect the volume of *X* chromosomes to shrink proportionally with the decrease in nuclear volume. We found that the volume of the *X* chromosomes does vary with nuclear size (Figure 4B), but as nuclear volume

decreases, the volume of the *X* chromosomes appears to decrease at a slower rate (Figure 4C). Therefore, although the *X* chromosomes get smaller as nuclei get smaller, they appear to occupy a larger proportion of the nucleus as nuclear volume decreases. Although the reason for this phenomenon is not known, its effects are averted in all analyses in two ways. First, embryos are compared only if they are approximately age-matched, and second, the percentage of nuclear volume occupied by DPY staining is expressed as a function of nuclear volume where appropriate. The effect could be caused by the fact that volume measurements become less accurate, and are more likely to be overestimated, as the size of an object decreases. Thus, smaller objects are subjected to a proportionally larger error in measurement than bigger objects. In addition, the different staining methods may affect the relative accuracy of measurements to different degrees depending on the object size.

The DCC recognizes and associates with the *X* duplication *mnDp10* but apparently does not spread onto adjacent autosomal regions: To determine if the dosage compensation complex recognizes and associates with sub-regions of the *X* chromosome, we compared the distribution of DPY staining in wild-type *XX* embryos and *XX* embryos that also contain two copies of an autosome-attached *X* duplication. We first assayed embryos carrying *mnDp10*, a duplication of the right ~30% of the *X* chromosome attached to the right end of chromosome *I* (HERMAN *et al.* 1979) (Figure 5).

We envisioned three possible outcomes in comparing *mnDp10*-bearing and wild-type embryos (Figure 5B). The first outcome is that the DCC can bind the duplication, and that the DPY-staining associated with the duplication can be resolved spatially from the *X* chromosomes. The second outcome is that the DCC can bind the duplication, but for technical or biological reasons cannot be resolved spatially from the *X*. The final outcome is that the DCC is unable to

bind the duplication, or we are unable to detect the binding. Two independent questions were asked to distinguish these outcomes: (1) Is there an increase in the number of DPY-staining bodies per nucleus in duplication-bearing strains? (2) Does total DPY-staining occupy a larger portion of the nuclear volume in duplication-bearing strains? The first outcome demands an affirmative answer to both questions, and would indicate that the autosome-attached duplication can be recognized as *X*-chromosome DNA. The second outcome predicts a negative answer to question one, but an affirmative answer to question two. Finally, a negative answer to both questions would indicate either that the duplication cannot be recognized as *X*-chromosome DNA, or that its size or brightness is below the physical limits of detection.

If the DCC binds the duplication and can be resolved from the *X* chromosomes, a third question would be asked to address whether the duplication acts as a nucleation center for DCC binding, which then spreads onto autosomal sequences: Is there a new class of DPY-staining bodies in duplication-bearing strains, and how large are these new bodies compared to a normal *X*? If the new DPY staining bodies are large (chromosome-sized) then the duplication may act as a nucleation center for DCC binding, with subsequent spreading into autosomal sequences. If the extra staining bodies are small (duplication-sized), then it is likely that only the duplication is recognized as *X*, and the binding does not spread a significant distance onto autosomal DNA.

(1) The number of DPY-staining bodies is increased per nucleus in *mnDp10*-bearing strains: The three histograms shown in Figure 6A-C, each representing an independent experiment, reveal a consistent increase in the number of DPY-staining bodies per nucleus in *mnDp10* strains. In each of the three experiments, a lower proportion of the *mnDp10* nuclei contain one staining body (53%, 51%, and 49%) compared to wild-type nuclei (66%, 62%, and 63% respectively). This difference exists because a higher proportion of *mnDp10* nuclei contain

two (34%, 41%, 38%) or three (12%, 8%, 10%) DPY-staining bodies compared to wild-type nuclei (two bodies: 30%, 33%, 33%; three bodies: 0.3%, 0.3%, 0.4%). These results suggest that DPY-27 and DPY-26 localize to *mnDp10*, and that this localization is manifested by the appearance of extra staining bodies. One might expect to see four DPY-staining bodies in nuclei that harbor an *X* duplication (the two *X*s and the two duplications). However, the appearance of any extra bodies would be obscured by the same factors that cause 65% of wild-type *XX* nuclei to be counted as having one body of DPY-staining. Furthermore, any additional DPY staining in the nuclei of *mnDp10* strains would further crowd the nucleus with fluorescence signal, making it even more difficult to resolve the additional *mnDp10* bodies. Considering these confounding factors, we interpret the consistently observed changes in the proportion of nuclei harboring multiple staining bodies to be significant. Therefore, an increase in the number of DPY-staining bodies per nucleus is observed in *mnDp10*-bearing embryos compared to wild-type embryos, consistent with a new, physically distinct target for the DCC.

(2) Total DPY-staining occupies a larger portion of the nuclear volume in *mnDp10*-bearing strains: If *mnDp10* is recognized by the dosage compensation complex, one would expect an increase in the total amount of DPY staining in each nucleus. Assuming that *mnDp10* is 30% of *X*, one would ideally expect DPY staining to occupy an additional ~3% of nuclear volume. In *mnDp10* strains, DPY-27 staining (Experiments 1 and 2, Table 1) occupied an additional 0.90% of the nuclear volume (wild-type, 10.06% \pm 0.08% standard error; *mnDp10*, 10.96% \pm 0.10%), representing an 8.9% increase ($p = 1.45 \times 10^{-12}$, two-tailed Student's *t*-test) compared to the expected 30%. In agreement with this increase, total DPY-26 staining (Experiments 3 and 4, Table 1) occupies an additional 1.05% of nuclear volume in *mnDp10* strains (wild-type, 14.11% \pm 0.09%; *mnDp10*, 15.15% \pm 0.13%), an increase of 7.4% ($p = 2.05 \times$

10^{-11} , t-test). This increase in total staining is reflected in the histograms shown in Figure 6D-E. These charts show the percentage of nuclear volume occupied by DPY staining (x axis) plotted against the percentage of nuclei containing that volume of staining (y axis). The distribution for *mnDp10* nuclei is shifted to the right, indicating an increase in total DPY-27 staining. For example, in Figure 6D every bin to the right of 12% contains more *mnDp10* nuclei, while every bin to the left of 12% contains more wild-type nuclei. The deviation from the ideal increase (~30%) in staining probably reflects the challenge of resolving *mnDp10* from the X chromosome in crowded nuclei (see also below).

The observed increase in the percentage of volume occupied is not a consequence of age differences between *mnDp10* embryos (average age, 139 cells) and wild-type embryos (average age, 154 cells), since for both DPY-26 and DPY-27 antibodies, *mnDp10* strains exhibit an increase in DPY-staining volume regardless of nuclear volume. This result is shown in Figure 7, where the percentage of nuclear volume occupied by DPY staining was plotted as a function of nuclear volume. The demonstrated increase in DPY staining in *mnDp10* nuclei indicates that the additional DPY-staining bodies found in *mnDp10* embryos arise from new target sequences, rather than from a physical reorganization of existing targets. Furthermore, the magnitude of the increase (~8%) suggests that *mnDp10* is represented by an additional small body of staining.

(3) A new class of small DPY-staining bodies exists in *mnDp10*-bearing

strains: To test the hypothesis that *mnDp10* is represented by an additional small body of DPY-staining, we recorded the volume occupied by individual DPY-staining bodies in wild-type and *mnDp10* nuclei. We then calculated the percentage of nuclear volume occupied by individual DPY-staining bodies. Histograms of the data (Figure 8) show a dramatic increase in the occurrence of small DPY-staining bodies in the *mnDp10* strain. We interpret the new class of

DPY-staining bodies to be *mnDp10*. Such a body can be visualized in the 3-D reconstruction shown in Figure 9.

We used the data from Experiment 1 (Figure 8A) to determine the properties of the new class of DPY-staining bodies. If *mnDp10* is defined conservatively as bodies occupying 0.2% to 2.2% of nuclear volume, an *mnDp10*-sized body was found in an average of 34.1% of *mnDp10* nuclei, compared to 13.0% of N2 nuclei, a 2.6 fold increase. Based on the appearance of the new class of DPY-staining bodies, *mnDp10* may also be defined in absolute terms as DPY-staining bodies ranging in volume from $35\text{-}400 \times 10^6 \text{ nm}^3$. To ascertain how reliably we could score the presence of *mnDp10*, we asked how often we could detect a joined *X* (defined as $> (1337 \times 10^6 \text{ nm}^3 - 1 \text{ SD})$) plus *mnDp10* (defined as a body of size $35\text{-}400 \times 10^6 \text{ nm}^3$) OR two *X* chromosomes (both $678 \times 10^6 \text{ nm}^3 \pm 1 \text{ SD}$) plus *mnDp10*. These conditions were satisfied in 27.1% of *mnDp10* nuclei and only 12.1% of N2 nuclei. Therefore, using these empirical definitions, we are able to detect the two *X* chromosomes and *mnDp10* in 27% of all *mnDp10* embryonic nuclei, with a false positive rate of 12%.

This low level of detection may be due to the crowding of fluorescence in the nucleus. In fact, this problem would be compounded by any additional DPY staining caused by *mnDp10*, making it likely that many *mnDp10* bodies are not resolved from each other or from the normal *X*-chromosome staining. A biological explanation may also exist: perhaps *mnDp10* is only recognized by the DCC a certain percentage of the time, or is recognized only in particular tissues. These factors, along with physical limits on the resolution of light microscopy and the small size of *C. elegans* nuclei (MATERIALS AND METHODS) conspire to make the detection of an extra staining body difficult, especially without an independent marker for the position of the duplication in the nucleus.

In nuclei interpreted to contain *mnDp10*, the DPY-staining that defines the duplication occupies an average of 1.06% of total nuclear volume, or $182 \times 10^6 \text{ nm}^3$. For comparison, the average volume of a single *X* is $678 \times 10^6 \text{ nm}^3$, indicating that *mnDp10* occupies on average 26.76% of the volume of a single *X* (data from Experiment 1, Table 1). Therefore, new DPY-staining bodies observed in the *mnDp10* strains occupy a small volume compared to the volume of the *X* chromosome, a result consistent with the dosage compensation machinery binding to *X* sequences but not spreading far onto adjacent autosomal sequences, if at all. This result demonstrates that the duplication contains all the information necessary to specify *X* identity and that the dosage compensation machinery can localize to a site distinct from the normal *X* chromosomes. However, this result does not rule out a spreading mechanism. Should spreading from a nucleation center be the means by which complexes extend along *X*, an *X* duplication must attach to an autosomal location that would block the spreading, otherwise the *X* duplication would cause reduced autosomal gene expression and probably death. Nonetheless, the absence of extensive spreading does support the hypothesis that a more evenly distributed *X*-recognition signal is required for the propagation of DCC binding.

***yDp14*, *stDp2*, and *mnDp27* embryos are indistinguishable from wild-type embryos:**

To examine other areas of the *X* chromosome for DCC-binding activity, we analyzed strains carrying either *yDp14*, a duplication of the left end of *X* that is also attached to chromosome *I*, *stDp2*, a duplication of the center of *X* integrated into chromosome *II*, or *mnDp27*, a duplication of the right end of *X* attached to the end of chromosome *II* (Figure 5).

To analyze *yDp14*, a total of 1759 nuclei from 10 embryos were examined (Table 1 and web supplement) using the same experimental tests and filtering conditions that were applied to the *mnDp10* embryos. Unlike *mnDp10* embryos, *yDp14* embryos showed no significant increase

in the number of DPY-27 staining bodies per nucleus (Figure 10A, Table 1). Overall, the same proportion of *yDp14* nuclei contained one (66%), two (31%), and three (3%) bodies of staining as wild-type nuclei (64%, 32%, and 4% respectively). In addition, no consistent increase in total DPY-staining volume was observed (Figure 10B and 10D). Finally, no new class of DPY-staining objects appeared in *yDp14* strains (Figure 10C). When the same analysis was applied to 3134 *stDp2* nuclei and 1374 *mnDp27* nuclei (Table 1 and web supplement), no significant deviation was seen from wild-type nuclei for any of the three aspects of staining that were measured. These results indicate that either the DCC cannot recognize *yDp14*, *stDp2*, and *mnDp27* as X-chromosome DNA, or that the size and intensity of the signal produced by the binding of the duplication falls below the limit of detection for this method.

X-chromosome DNA has 14 families of X-enriched sequence elements: In *mnDp10* embryos, the failure of the DCC to spread from X sequences to autosomal sequences suggests that *C. elegans* X-recognition elements may be widely distributed across the X. Therefore, spreading might not have to occur over large distances. To identify potential X-recognition elements, we analyzed the *C. elegans* genome sequence (99% complete) using a computational approach. Our goal was to identify repeated X-enriched sequence strings that may act as X-recognition elements. We wrote a program called “count” that can determine the frequency of every string of length N that occurs on a chromosome, where N is any number supplied by the user. To find X-enriched sequences, we used this program to look for nonamers that occur more than 75 times on X and occur at least ten times more frequently on X than on the autosomes (Table 2, see MATERIALS AND METHODS for details). The 58 nonamers that meet these criteria are listed in Table 2. A string length of nine was found to produce the most informative results. Shorter strings occur too often by chance (they are “noisy”), and we found that 9 bp queries were

able to detect much longer repeat units, since units longer than 9 bp will also contain a repeating unit of 9 bp.

To determine which of the nonamers were members of a common family of *X*-enriched elements, we wrote a program that maps the position of strings onto any sequence file (MATERIALS AND METHODS). We reasoned that strings representing the same repeating unit could be sorted into families by determining which of them have similar distribution patterns. By comparing the distribution patterns of the 58 selected strings, 14 families of *X*-enriched sequences were identified (Table 3). We found that these 14 families could be further divided into one group of six, whose repeat elements were concentrated in tight clusters on the *X* chromosome (Figure 11), and one group of eight, whose repeated elements were more evenly dispersed across the *X* (Figure 12). The distribution patterns of the *X*-enriched sequence families are diverse, ranging from the majority of occurrences on a single cosmid to a roughly even spacing along the *X*-chromosome. By manual inspection, the true repeating unit of each of the families was found to range from 32 base pairs to 226 base pairs (Table 3). The *mnDp10* results suggest that *X*-enriched sequence families that occur in a very confined region of *X* are less likely to be *X*-recognition elements. The remaining "unclustered" candidate *X*-recognition sequences provide a solid starting point for further dissection of the *cis*-acting elements that determine the binding specificity of the dosage compensation complex.

To test the biological significance of the *X*-enriched repeats, complementary oligonucleotides specific for the repeating unit of each family were synthesized, the oligos were annealed to form duplex DNA, and the resulting double-stranded DNAs were assayed for DCC binding activity in the *lacI/lacO* array-based system (MATERIALS AND METHODS; DAWES *et al.* 1999). Of the 15 oligonucleotide pairs tested for activity, all gave a negative result. Future

experiments will examine each of the repeat sequences in the context of larger segments of *X* DNA to determine whether they are necessary, but just not sufficient to recruit the dosage compensation machinery.

DISCUSSION

Our work leads to important conclusions regarding the mechanism used by the dosage compensation machinery of *C. elegans* to recognize *X* chromosomes. We have shown that the dosage compensation machinery can assemble on a site distinct from the full-length *X* chromosome, namely on a partial duplication of *X* that has been removed from its normal chromosomal context through its linkage to an autosome. Therefore, a discrete portion of *X* can retain its identity as *X* and its ability to recruit the dosage compensation machinery. In our experiments, the dosage compensation machinery appears not to have spread far, if at all, onto adjacent autosomal sequences. The lack of significant spreading suggests that *X*-chromosome recognition and DCC binding in *C. elegans* may not proceed via the mechanism used by mammals to inactivate their *X* chromosome: nucleation and spreading from a single site. It is more likely that either no spreading occurs in *C. elegans*, or that limited spreading occurs from several chromatin entry sites, as proposed for *Drosophila*. However, in view of the caveats discussed below, it remains possible that the *X* chromosome contains a single site for binding the DCC complex, and the transcriptional repression spreads from there.

The initial suggestion that *X*-chromosome duplications might compete with the normal *X* chromosome for dosage compensation proteins came over 12 years ago with a study showing that *X*-chromosome duplications affect the expression of *X*-linked genes that were not duplicated (MENEELY and NORDSTROM 1988). In that study, the phenotype caused by an *X*-linked

hypomorphic *lin-15* mutation was partially suppressed by *mnDp25* and *stDp2*, suggesting that expression of *lin-15* could be increased without increasing its gene copy number. This conclusion was corroborated by an assay that demonstrated an increase in the enzymatic activity of the X-linked acetylcholinesterase gene *ace-1*, also not duplicated by *mnDp25* or *stDp2*. *mnDp10* was not examined, because it covers both loci. However, in a separate study using northern blots as a direct measure of gene activity, *mnDp10* was shown to increase the mRNA levels of *uvt-4* and *uxt-1*, two X-linked loci not duplicated by *mnDp10* (B. J. M., UNPUBLISHED DATA.).

Both sets of experiments were conducted before the discovery of the dosage compensation complex, and it was not possible then to distinguish between two competing hypotheses. The first hypothesis was that the duplications titrated a repressor of gene expression away from X, while the second contended that the duplications contained wild-type copies of one or more general enhancers of X-linked gene expression, or less likely enhancers of the specific loci tested. Increased gene expression might also have arisen from other physiological perturbations caused by the duplication. Experiments have since shown that the DCC binds to X (CHUANG *et al.* 1994; CHUANG *et al.* 1996; LIEB *et al.* 1996; LIEB *et al.* 1998), but whether the DCC is capable of binding to X-chromosome duplications had not been determined. Therefore, the results presented here permit us to interpret the previous duplication experiments in a new light, and to conclude that the repressive dosage compensation machinery can be titrated away from X by a duplication. The combination of results also implies that at least one DCC component is limiting for full dosage compensation function.

Do X-chromosome duplications make good models for the behavior of X chromosomes during dosage compensation? Valid concerns temper the conclusions that can be made based on

the DCC-binding properties of *mnDp10*. Any duplication that could act as a nucleation site for the spreading of the DCC onto an autosome would be expected to cause hermaphrodite lethality. Presumably, such duplications would be selected against during the isolation procedure, and therefore only duplications that fail to act as centers for nucleation and spreading would have arisen. This concern is heightened by the unusual number of duplications attached to the right end of chromosome *I*, suggesting that some selection for that attachment point occurred. One possibility is that the presence of the 28S *rDNA* repeat cluster at the right end of chromosome *I* might preclude spreading and therefore select for the attachment of *X* duplications adjacent to it.

These caveats are difficult to address directly. Unfortunately, for the analysis presented here, it was essential that the partial *X* duplications be physically attached to an autosome, because unattached duplications are not mitotically stable, and their loss during embryonic development is difficult to monitor. In addition, only strains that are viable as duplication homozygotes are amenable to analysis because no practical way exists in our assay to distinguish among embryos with zero, one, or two copies of the duplication. These restrictions sharply reduce the number of duplications available for study. Furthermore, chromosomal duplications are created essentially at random by irradiation, making it difficult to create “custom” duplications or attachment points. Two of the duplications analyzed in this study, *stDp2* and *mnDp27*, were chosen because they are not attached to chromosome *I* and do not cause lethality when homozygosed. However, both duplications produced negative results.

These negative results may be due to the biological inability of the DCC to bind these duplications, or to the technical limitations of our assay system. When interpreting the negative results, it is important to consider the positive case, *mnDp10*. For *mnDp10* strains, we estimated that only one in four nuclei contained an independent DPY-staining body that could be scored as

mnDp10, and this number drops to only 15% if false positives are subtracted. *mnDp10* is the largest of the *X* duplications examined, and it stands to reason that smaller duplications might be detected less frequently by our assay. Therefore, negative results do not rule out the possibility that the DCC can bind to the duplications *in vivo*.

The work presented here provides a solid foundation for addressing important unanswered questions regarding the mechanism of *X*-chromosome recognition in *C. elegans*. A pressing challenge is to determine the precise nature of the DNA elements that specify *X*-chromosome identity. In principle, the features that distinguish *X* chromosomes from autosomes might include specific repeated *X*-DNA sequences or *X*-specific DNA structures. Alternatively, instead of recruitment factors on *X*, repelling factors might exist on autosomes to prevent the dosage compensation machinery from binding. Although our experiments do not discriminate among these possibilities, they do indicate that the DCC can assemble on *X* DNA sequences removed from the context of the entire *X* chromosome, implying that further investigations using the GFP-tagged artificial-chromosome assay to delineate candidate *X*-recognition sequences may prove fruitful.

Important leads in the search for *X*-recognition elements may also emerge from the fourteen families of *X*-enriched sequence elements that were discovered and mapped onto the *X* chromosome. The similarity between *C. elegans* dosage compensation proteins and general mitotic factors in worms and other organisms suggests that understanding further how *X* is distinguished from the autosomes in *C. elegans* will reveal fundamental properties of chromatin recognition by more general factors.

ACKNOWLEDGEMENTS

We thank Aaron Straight for providing the *lacO* repeat plasmid pSV2-dhFr8.32 used in the array studies and Aidyl Gonzalez-Serricchio for providing plasmid pPD49-78, which expresses *lacI-gfp* under the control of the *hsp-16* heat-shock promoter. We are grateful to Donna Albertson for advice concerning microscopy.

LITERATURE CITED

- AMREIN, H., and R. AXEL, 1997 Genes Expressed in Neurons of Adult Male *Drosophila*. *Cell* **88**: 459-469.
- BASHAW, G. J., and B. S. BAKER, 1995 The *msl-2* dosage compensation gene of *Drosophila* encodes a putative RNA-binding protein whose expression is sex specifically regulated by *Sex-lethal*. *Development* **121**: 3245-3258.
- BHADRA, U., M. PAL-BHADRA and J. A. BIRCHLER, 1999 Role of the *male specific lethal (msl)* genes in modifying the effects of sex chromosomal dosage in *Drosophila*. *Genetics* **152**: 249-68.
- BHAT, M. A., A. V. PHILIP, D. M. GLOVER and H. J. BELLEN, 1996 Chromatid Segregation at Anaphase Requires the barren Product, a Novel Chromosome-Associated Protein That Interacts with Topoisomerase II. *Cell* **87**: 1103-1114.
- BONE, J. R., and M. I. KURODA, 1996 Dosage compensation regulatory proteins and the evolution of sex chromosomes in *Drosophila*. *Genetics* **144**: 705-13.
- BRENNER, S., 1974 The genetics of *Caenorhabditis elegans*. *Genetics* **77**: 71-94.
- BROWN, C. J., and H. F. WILLARD, 1994 The human X-inactivation centre is not required for maintenance of X-chromosome inactivation. *Nature* **368**: 154-6.

- CARMI, I., J. B. KOPCZYNSKI and B. J. MEYER, 1998 The nuclear hormone receptor SEX-1 is an *X*-chromosome signal that determines nematode sex [see comments]. *Nature* **396**: 168-73.
- CHUANG, P.-T., D. G. ALBERTSON and B. J. MEYER, 1994 DPY-27: a chromosome condensation protein homolog that regulates *C. elegans* dosage compensation through association with the *X* chromosome. *Cell* **79**: 459-474.
- CHUANG, P.-T., J. D. LIEB and B. J. MEYER, 1996 Sex-specific assembly of a dosage compensation complex on the nematode *X* chromosome. *Science* **274**: 1736-1739.
- CLEMONS, C. M., J. A. MCNEIL, H. F. WILLARD and J. B. LAWRENCE, 1996 *XIST* RNA paints the inactive *X* chromosome at interphase: evidence for a novel RNA involved in nuclear/chromosome structure. *J. Cell Biol.* **132**: 259-275.
- CLINE, T. W., and B. J. MEYER, 1996 Vive la différence: males vs. females in flies vs. worms. *Annu. Rev. Genet.* **30**: 637-702.
- Csankovszki, G., B. Panning, B. Bates, J. R. Pehrson and R. Jaenisch, 1999 Conditional deletion of *Xist* disrupts histone macroH2A localization but not maintenance of *X* inactivation. *Nature Genetics* **22**: 323-4.
- DAVIS, T. L., and B. J. MEYER, 1997 SDC-3 coordinates the assembly of a dosage compensation complex on the nematode *X* chromosome. *Development* **124**: 1019-1031.
- DAWES, H. E., D. S. BERLIN, D. M. LAPIDUS, C. NUSBAUM, T. L. DAVIS *et al.*, 1999 Dosage compensation proteins targeted to *X* chromosomes by a determinant of hermaphrodite fate [see comments]. *Science* **284**: 1800-4.
- DEAN, P., L. MASCIIO, D. OW, D. SUDAR and J. MULLIKIN, 1990 Proposed standard for image cytometry data files. *Cytometry* **11**: 561-9.

- DELONG, L. D., J. D. PLENEFISCH, R. D. KLEIN and B. J. MEYER, 1993 Feedback control of sex determination by dosage compensation revealed through *Caenorhabditis elegans* *sdC-3* mutations. *Genetics* **133**: 875-896.
- GORMAN, M., A. FRANKE and B. S. BAKER, 1995 Molecular characterization of the *male-specific lethal-3* gene and investigation of the regulation of dosage compensation in *Drosophila*. *Development* **121**: 463-475.
- GORMAN, M., M. I. KURODA and B. S. BAKER, 1993 Regulation of the sex-specific binding of the *maleless* dosage compensation protein to the male X chromosome in *Drosophila*. *Cell* **72**: 39-49.
- GU, W., P. SZAUTER and J. C. LUCCHESI, 1998 Targeting of MOF, a putative histone acetyl transferase, to the X chromosome of *Drosophila melanogaster*. *Dev. Genet.* **22**: 56-64.
- HERMAN, R. K., J. E. MADL AND C. K. KARI, 1979 Duplications in *Caenorhabditis elegans*. *Genetics* **92**: 419-435.
- HERZING, L. B. K., J. T. ROMER, J. M. HORNE and A. ASHWORTH, 1997 *Xist* has properties of the X-chromosome inactivation centre. *Nature* **386**: 272-275.
- HIRANO, T., KOBAYASHI, R., and M. HIRANO, 1997 Condensins, chromosome condensation protein complexes containing XCAP-C, XCAP-E and a *Xenopus* homolog of the *Drosophila* Barren protein. *Cell* **89**:511-521.
- HIRANO, T. 1999 SMC-mediated chromosome mechanics: a conserved scheme from bacteria to vertebrates? *Genes Dev.* **13**: 11-19.
- HODGKIN, J., 1983 X chromosome dosage and gene expression in *Caenorhabditis elegans*: two unusual dumpy genes. *Mol. Gen. Genet.* **192**: 452-458.

- HSU, D. R., P.-T. CHUANG and B. J. MEYER, 1995 DPY-30, a nuclear protein essential early in embryogenesis for *Caenorhabditis elegans* dosage compensation. *Development* **121**: 3323-3334.
- JEPPESEN, P., and B. M. TURNER, 1993 The inactive X chromosome in female mammals is distinguished by a lack of histone H4 acetylation, a cytogenetic marker for gene expression. *Cell* **74**: 281-289.
- KELLEY, R. L., I. SOLOVYEVA, L. M. LYMAN, R. RICHMAN, V. SOLOVYEV *et al.*, 1995 Expression of MSL-2 causes assembly of dosage compensation regulators on the X chromosomes and female lethality in *Drosophila*. *Cell* **81**: 867-877.
- KELLEY, R. L., V. H. MELLER, P. R. GORDADZE, G. ROMAN, R. DAVIS *et al.*, 1999 Epigenetic Spreading of the *Drosophila* Dosage Compensation Complex from *roX* RNA Genes into Flanking Chromatin. *Cell* **98**: 513-522.
- KLEIN, R. D., and B. J. MEYER, 1993 Independent domains of the *sdc-3* protein control sex determination and dosage compensation in *C. elegans*. *Cell* **72**: 349-364.
- KOSHLAND, D. AND A. STRUNNIKOV, 1996 Mitotic Chromosome Segregation. *Ann. Rev. Cell Dev. Biol.* **12**: 305-333.
- KURODA, M. I., M. J. KERNAN, R. KREBER, B. GANETZKY and B. S. BAKER, 1991 The *maleless* protein associates with the X chromosome to regulate dosage compensation in *Drosophila*. *Cell* **66**: 935-947.
- LEE, J. T., and R. JAENISCH, 1997 The (epi)genetic control of mammalian X-chromosome inactivation. *Curr. Opin. Genet. Dev.* **7**: 274-80.
- LEE, J. T., and N. LU, 1999 Targeted mutagenesis of *Tsix* leads to nonrandom X inactivation. *Cell* **99**: 47-57.

- LEE, J. T., N. LU and Y. HAN, 1999 Genetic analysis of the mouse X inactivation center defines an 80-kb multifunction domain. *Proc. Natl. Acad. Sci. USA* **96**: 3836-41.
- LEE, J. T., W. M. STRAUSS, J. A. DAUSMAN and R. JAENISCH, 1996 A 450 kb transgene displays properties of the mammalian X-inactivation center. *Cell* **86**: 83-94.
- LIEB, J. D., M. R. ALBRECHT, P. T. CHUANG and B. J. MEYER, 1998 MIX-1: an essential component of the *C. elegans* mitotic machinery executes X chromosome dosage compensation. *Cell* **92**: 265-77.
- LIEB, J. D., E. E. CAPOWSKI, P. MENEELY and B. J. MEYER, 1996 DPY-26, a link between dosage compensation and meiotic chromosome segregation in the nematode. *Science* **274**: 1732-1736.
- LYMAN, L. M., K. COPPS, L. RASTELLI, R. L. KELLEY and M. I. KURODA, 1997 *Drosophila male-specific lethal-2* protein: structure/function analysis and dependence on MSL-1 for chromosome association. *Genetics* **147**: 1743-53.
- LYON, M. F., 1961 Gene action in the X chromosome of the mouse (*Mus musculus* L.). *Nature* **190**: 372-373.
- MALPICA, N., C. O. DE SOLORZANO, J. J. VAQUERO, A. SANTOS, I. VALLCORBA *et al.*, 1997 Applying watershed algorithms to the segmentation of clustered nuclei. *Cytometry* **28**: 289-97.
- MARAHRENS, Y., J. LORING and R. JAENISCH, 1998 Role of the *Xist* gene in X chromosome choosing. *Cell* **92**: 657-64.
- MELLER, V. H., 2000 Dosage compensation: making 1X equal 2X. *Trends Cell Biol.* **10**: 54-9.

- MELLER, V. H., K. H. WU, G. R. ROMAN, M. I. KURODA and R. L. DAVIS, 1997 *roXI* RNA Paints the X Chromosome of Male *Drosophila* and Is Regulated by the Dosage Compensation System. *Cell* **88**: 445-457.
- MENEELY, P. M., and K. D. NORDSTROM, 1988 X chromosome duplications affect a region of the chromosome they do not duplicate in *Caenorhabditis elegans*. *Genetics* **119**: 365-75.
- MEYER, B., 2000 Sex in the worm: counting and compensating X-chromosome dose. *Trends in Genetics* **16**: 247-253.
- MEYER, B. J., 1997 Sex Determination and X Chromosome Dosage Compensation, pp. 209-240 in *C. elegans II*, edited by T. B. D. L. Riddle, B. J. Meyer and J. R. Priess. Cold Spring Harbor Press, Cold Spring Harbor, New York.
- MEYER, B. J., and L. P. CASSON, 1986 *Caenorhabditis elegans* compensates for the difference in X chromosome dosage between the sexes by regulating transcript levels. *Cell* **47**: 871-881.
- MOHANDAS, T., R. S. SPARKES and L. J. SHAPIRO, 1981 Reactivation of an inactive human X chromosome: evidence for X inactivation by DNA methylation. *Science* **211**: 393-396.
- NUSBAUM, C., and B. J. MEYER, 1989 The *Caenorhabditis elegans* gene *sdc-2* controls sex determination and dosage compensation in XX animals. *Genetics* **122**: 579-593.
- ORTIZ DE SOLORZANO, C., E. GARCIA RODRIGUEZ, A. JONES, D. PINKEL, J. W. GRAY *et al.*, 1999 Segmentation of confocal microscope images of cell nuclei in thick tissue sections. *J. Microsc.* **193**: 212-26.
- ORTIZ DE SOLORZANO, C., A. SANTOS, I. VALLCORBA, J. M. GARCIA-SAGREDO and F. DEL POZO, 1998 Automated FISH spot counting in interphase nuclei: statistical validation and data correction. *Cytometry* **31**: 93-9.

- PALMER, M. J., V. A. MERGNER, R. RICHMAN, J. E. MANNING, M. I. KURODA *et al.*, 1993 The *male-specific lethal-one (msl-1)* gene of *Drosophila melanogaster* encodes a novel protein that associates with the X chromosome in males. *Genetics* **134**: 545-557.
- PALMER, M. J., R. RICHMAN, L. RICHTER and M. I. KURODA, 1994 Sex-specific regulation of the *male-specific lethal-1* dosage compensation gene in *Drosophila*. *Genes Dev.* **8**: 698-706.
- PENNY, G. D., G. F. KAY, S. A. SHEARDOWN, S. RASTAN and N. BROCKDORFF, 1996 Requirement for *Xist* in X-chromosome inactivation. *Nature* **379**: 131-137.
- PLENEFISCH, J. D., L. DELONG and B. J. MEYER, 1989 Genes that implement the hermaphrodite mode of dosage compensation in *Caenorhabditis elegans*. *Genetics* **121**: 57-76.
- STRAIGHT, A., A. BELMONT, C. ROBINETT and A. MURRAY, 1996 GFP tagging of budding yeast chromosomes reveals that protein-protein interactions can mediate sister chromatid cohesion. *Cur. Biol.* **6**: 1599-608.
- THE *C. ELEGANS* SEQUENCING CONSORTIUM, 1998 Genome Sequence of the Nematode *C. elegans*: A platform for investigating biology. *Science* **282**: 2012-2018.
- ZHOU, S., Y. YANG, M. J. SCOTT, A. PANNUTI, K. C. FEHR *et al.*, 1995 *Male-specific lethal 2*, a dosage compensation gene of *Drosophila* undergoes sex-specific regulation and encodes a protein with a RING finger and a metallothionein-like cysteine cluster. *EMBO J.*: 2884-2895.

TABLE LEGENDS

TABLE 1. Quantitative data summary

†† DPY-27 antibodies were used in Experiments 1 and 2, and DPY-26 antibodies were used in experiments 3 and 4. Due to differences between the microscopes and/or the antibodies, volume measurements from experiments 1 and 2 cannot be compared directly with those from experiments 3 and 4.

TABLE 2. Nonamers that occur more than 75 times on *X* and occur at least 10 times more frequently on *X* than on the autosomes

Shown in bold are the actual sequences whose *X*-chromosome distributions are in shown in Figures 11 and 12.

TABLE 3. Repeat families derived from *X*-enriched nonamers

“Approximate True Repeat Unit” and “Approximate True Repeat Length” were determined by manual examination of the *X* chromosome sequence near the positions reported by the 9mer map. Therefore, variations of the stated consensus may be present in any particular repeat unit. CeRep27 is reported to be excluded from introns (THE *C. ELEGANS* SEQUENCING CONSORTIUM 1998).

FIGURE LEGENDS

FIGURE 1.- A model for assembly of the dosage compensation complex on hermaphrodite *X* chromosomes in *C. elegans*. (A) In *XX* hermaphrodites, SDC-2 acts in conjunction with SDC-3 to activate dosage compensation by localizing a protein complex composed of DPY-26, DPY-27, DPY-28, and MIX-1 to both hermaphrodite *X* chromosomes. The end result is an approximately 2-fold reduction in *X*-linked gene expression from each *X* chromosome. (B) In *XO* males, the dosage compensation complex (DCC) is prevented from associating with *X* because the male-specific *xol-1* gene represses *sdc* gene activity. *X*-linked genes are fully expressed because the dosage compensation proteins are prevented from localizing to the single *X*.

FIGURE 2.- Three-dimensional (3-D) reconstruction of fluorescence in wild-type embryonic nuclei. (A-C) The 3-D reconstruction of anti-DPY-27 staining in a single nucleus. The black plane is a single section of original confocal data, and the blue objects are renderings based on the position of the edges of fluorescence in stacks of optical sections. The algorithms used to render and segment the DPY-27-labeled *X* chromosomes produced a 3-D body that was representative of the original data. All transformations of the raw confocal data (image filters, interpolation, and settings used for rendering) were identical for all samples analyzed in this paper. (D-F) Rendering of the DNA stain propidium iodide. daVinci, the software used to render the nuclei, allows one to adjust the opacity of the rendered DNA stain, permitting one to visualize the position of staining bodies inside the nuclei. (D) 0% opacity, (E) 25% opacity, (F) 100% opacity. (G-I) Sub-chromosomal pieces of DNA can be detected and resolved from the *X* chromosomes. (G) A wild-type embryo harboring an array composed of the *lacO*, *lacI-GFP*, and *rol-6* plasmids was stained with anti-GFP (FITC, green), anti-DPY-27 (CY5, red), and DAPI

(blue). A merged image of a single optical section is shown. (H-I) 3-D reconstructions of extra-chromosomal arrays (red), DPY-27-stained *X* chromosomes (dark blue) and DAPI staining (light blue) from two individual nuclei are shown. This embryo had 179 nuclei and 220 arrays. Fourteen (7.8%) nuclei contained zero arrays, 115 (64.2%) nuclei contained one array, 45 (25.1%) nuclei contained two arrays, and 5 (2.8%) nuclei contained three arrays. (J) The two *X* chromosomes often appear as one body of staining. These three nuclei are examples in which the two *X* chromosomes are counted as one staining body. *C. elegans* embryonic nuclei are generally 1-2 μm in diameter.

FIGURE 3. - In many nuclei, one body of DPY staining represents both *X* chromosomes. (A) A histogram showing that the DPY-27-staining bodies in nuclei containing one body are larger than the DPY-27-staining bodies in nuclei containing two bodies. Overall, the average size of a “disjoined” *X* was $678 \times 10^6 \text{ nm}^3$, about half the volume of a “joined” *X* (avg. $1338 \times 10^6 \text{ nm}^3$). (B) A histogram showing that DPY-27 staining occupies a similar volume regardless of whether the *X* chromosomes are resolved into one or two bodies. On average, the *X* occupied 10.2% of nuclear volume (avg. $1338 \times 10^6 \text{ nm}^3$) in nuclei with one body, and 9.3% of nuclear volume (avg. $1368 \times 10^6 \text{ nm}^3$) in nuclei with multiple bodies. The histograms in A and B are derived from wild-type embryos analyzed in Experiment 1 of Table 1 (1006 nuclei).

FIGURE 4.- Properties of wild-type nuclei and *X* chromosomes during embryonic development. (A) Average nuclear volume decreases as embryos develop. In both wild-type embryos (closed black diamonds, black line, $n=27$) and *mnDp10* embryos (open

squares, dashed line, n=22), as cell number increases, the average volume of the nuclei decreases. *mnDp10* is a duplication of the right end of *X* attached to chromosome I (See Figure 5). (B) The volume of the *X* chromosome decreases with the decrease in nuclear size. All data are from wild-type (N2) embryos (n=27). Each data point represents an average value from a single embryo. Data from two different antibodies, anti-DPY-26 (n=14, open squares, dashed line, acquired with a Leica confocal microscope) and anti-DPY-27 (n=13, closed black diamonds, solid line, acquired with a Zeiss confocal microscope) are shown. The DPY-26/Leica experiments consistently produced higher *X*-chromosome volume measurements. Whether this observation is biologically relevant, a property of the particular antibody used, or a property of the microscope that was used has not been determined. Despite the difference in absolute volume observed between DPY-26 and DPY-27 antibodies, the relative decrease in *X* volume with decreasing nuclear size is similar in the two data sets. (C) As nuclear volume decreases, the *X*-chromosomes appear to occupy a larger percentage of nuclear volume.

FIGURE 5.- The strategy and tools for examining *X*-chromosome duplications (A) A map of selected *X*-chromosome duplications. The name of the duplication is in italics, followed by its chromosomal attachment point (f = free), the number of genetic map units (mu) covered, and the approximate percentage of the *X* chromosome covered. Percentages may be overestimates, since coverage is defined genetically and some duplications contain uncharacterized internal deletions. *mnDp10* is known to have large deletions left of *unc-9* (map position 11.6): *unc-58* (1.50) and *unc-115* (1.7) are covered by *mnDp10*, but *dpy-22* (1.99), *vab-3* (2.01), and *lin-14* (3.48) are not. Although the precise extent of the deletions is not known, we estimate that *mnDp10* covers

~30% of X based on the available map data. Duplications in black were tested for DCC binding activity in this study. (B) A schematic representation of a wild-type karyotype and an *mnDp10* karyotype.

FIGURE 6.- *mnDp10* embryos have more individual DPY-staining bodies per nucleus than wild-type embryos, and total DPY staining occupies a greater percentage of the nuclear volume. (A-C) Number of DPY-staining bodies per nucleus compared in wild-type (black) and *mnDp10* (red) nuclei. (D-E) Volume of DPY-staining bodies compared in *mnDp10* and wild-type nuclei. These histograms show the percentage of nuclear volume occupied by DPY staining on the x axis, with the percent nuclei containing that volume of staining on the y axis. The distribution of *mnDp10* nuclei shows a pronounced shift to the right, indicating an increase in total DPY-27 staining. In (D), this difference occurs despite a higher average age for wild-type embryos (135 cells) compared to *mnDp10* embryos (114 cells). For (E) average ages were 161 cells for wild-type embryos and 171 cells for *mnDp10* embryos.

FIGURE 7.- In *mnDp10* embryos, DPY-staining occupies a greater percentage of the nuclear volume, regardless of nuclear size. (A) The average percentage of nuclear volume occupied by DPY-26 staining is plotted against average nuclear volume for *mnDp10* embryos (n=10) and wild-type embryos (n=14). Each data point represents the average values for a single embryo. (B) Same as for (A), but with anti-DPY-27 stained *mnDp10* embryos (n=13) and wild-type embryos (n=13).

FIGURE 8.- A new class of small DPY-staining bodies is present in *mnDp10* embryos. In each of the three histograms, the percentage of nuclear volume occupied by individual DPY-staining bodies is plotted on the x axis for both wild-type (black) and *mnDp10* (red) nuclei. The y axis shows the percent of all nuclei that contain a body of the size indicated on the x axis. In *mnDp10* strains, there is a marked increase in the number of staining bodies that occupy less than ~2.5% of nuclear volume.

FIGURE 9.- Visualization of *mnDp10*. (A-C) Volume rendering of a nucleus containing *mnDp10* stained with propidium iodide (light blue) and anti-DPY-27 antibody (dark blue). An X points to the X chromosomes, and the D points to the small piece of DPY-27 staining that we interpret to be *mnDp10*. Overall, it is estimated that both X chromosomes and an *mnDp10* staining body can be identified in 27% of all *mnDp10* nuclei (see text for explanation). The black plane shows an individual section of the original confocal data from the anti-DPY-27 channel.

FIGURE 10.- DPY staining in *yDp14* nuclei is not significantly different from DPY staining in wild-type nuclei. (A) No increase is found in the number of DPY-staining bodies in *yDp14* embryos. On average, *yDp14* nuclei contained 1.37 bodies per nucleus, compared to 1.42 bodies per nucleus for wild-type and 1.63 for *mnDp10* embryos. (B) DPY-staining occupies a similar volume in wild-type and *yDp14* embryos. (C) No new class of DPY-staining bodies exists in *yDp14* embryos. (D) No increase is observed in the proportion of the nuclear volume occupied in *yDp14* strains, regardless of nuclear volume. The average percentage of nuclear volume occupied by DPY-staining is plotted against average nuclear volume for *yDp14* embryos (open squares, dashed line) and wild-type embryos (closed diamonds, solid line). Each data point

represents the average values for a single embryo. Unlike *mnDp10* embryos (FIGURE 7), the trendline calculated for these duplication-bearing embryos is very close to the trendline for wild-type embryos. All data shown in this figure are from experiment 3. These data are representative of the negative results observed for *stDp2* and *mnDp27* (for data, see <http://www.genetics.org>).

FIGURE 11.- The X-chromosome distribution of clustered X-enriched motifs. The positions of a representative member of each family of clustered X-enriched sequences are shown as a histogram. Numbers on the x axis represent the location in base pairs ($\times 10^5$). Bars represent number of occurrences in each 10,000 bp bin. The actual sequence mapped for each sequence family is shown in bold in Table 2.

FIGURE 12.- The X-chromosome distribution of unclustered X-enriched motifs. The positions of a representative member of each family of unclustered X-enriched sequences are shown as a histogram. Numbers on the x axis represent the location in base pairs ($\times 10^5$). Bars represent number of occurrences in each 10,000 bp bin. The actual sequence mapped for each sequence family is shown in bold in Table 2.

FIGURES

Figure 1.

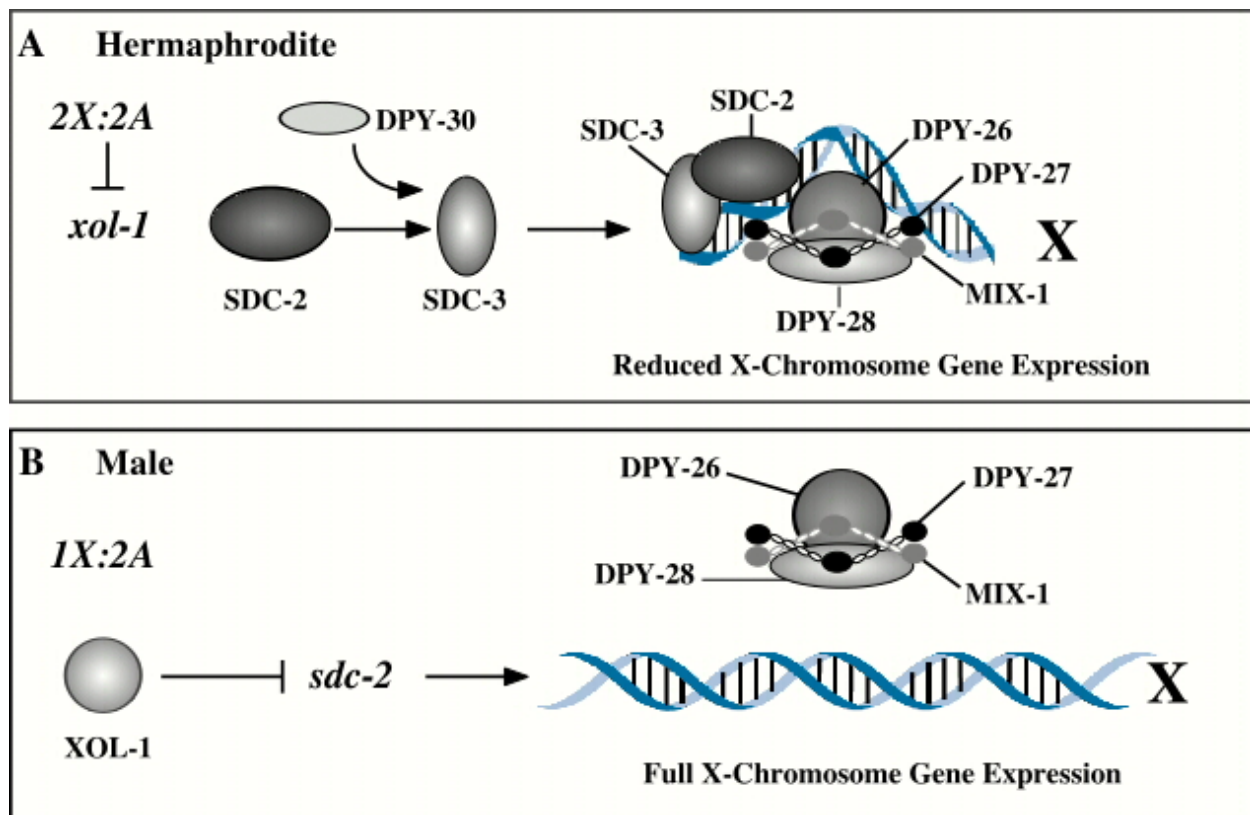


Figure 2

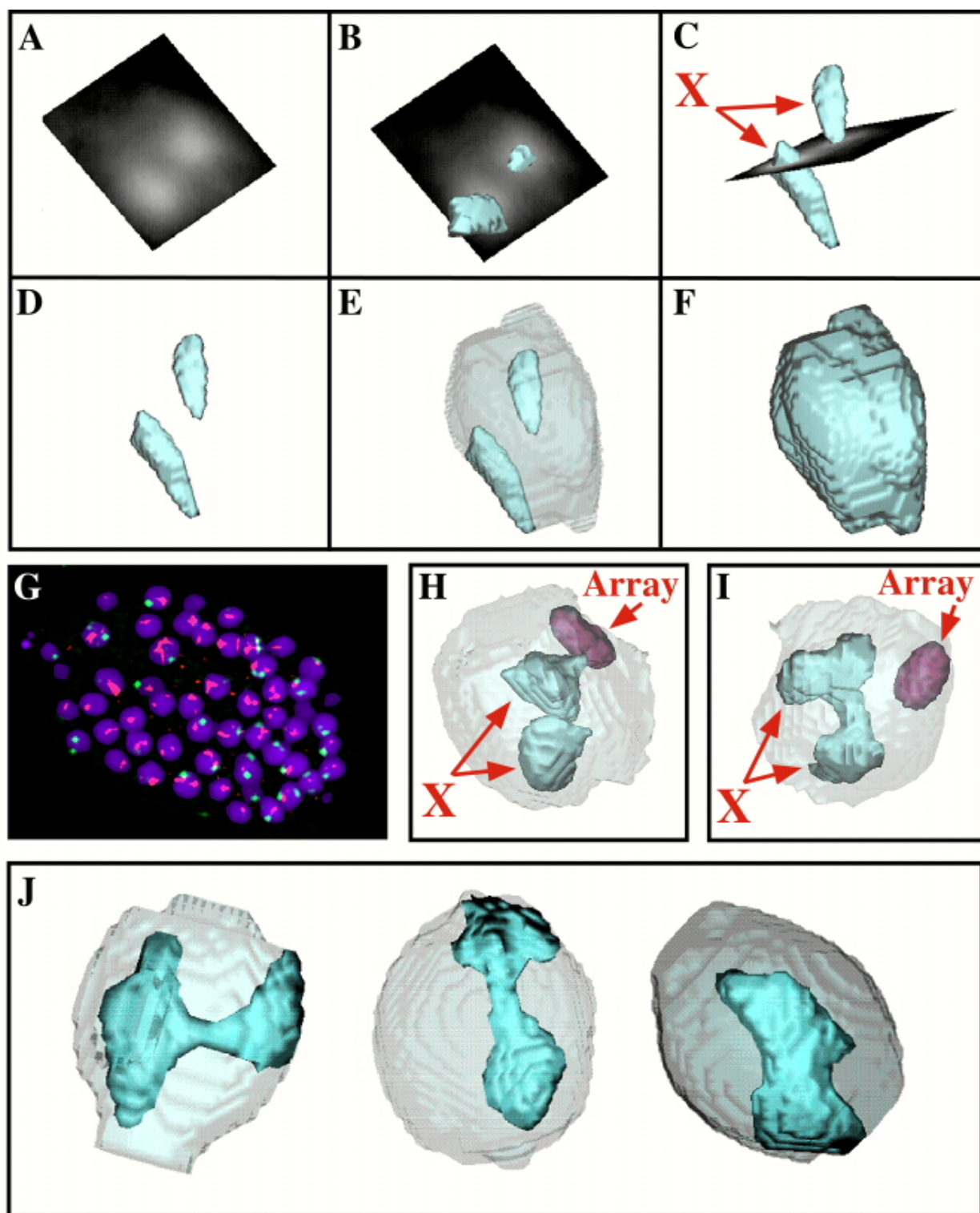


Figure 3.

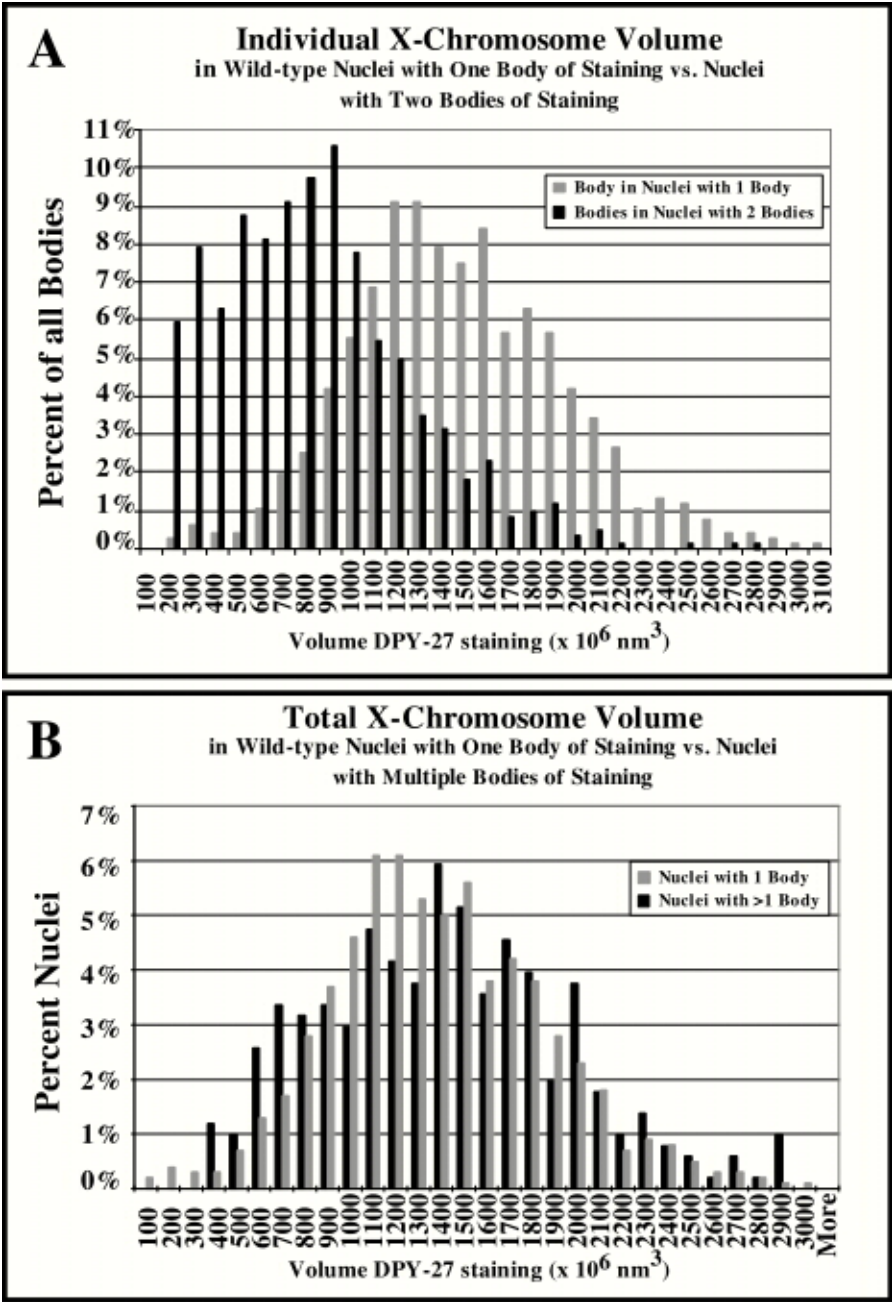


Figure 4.

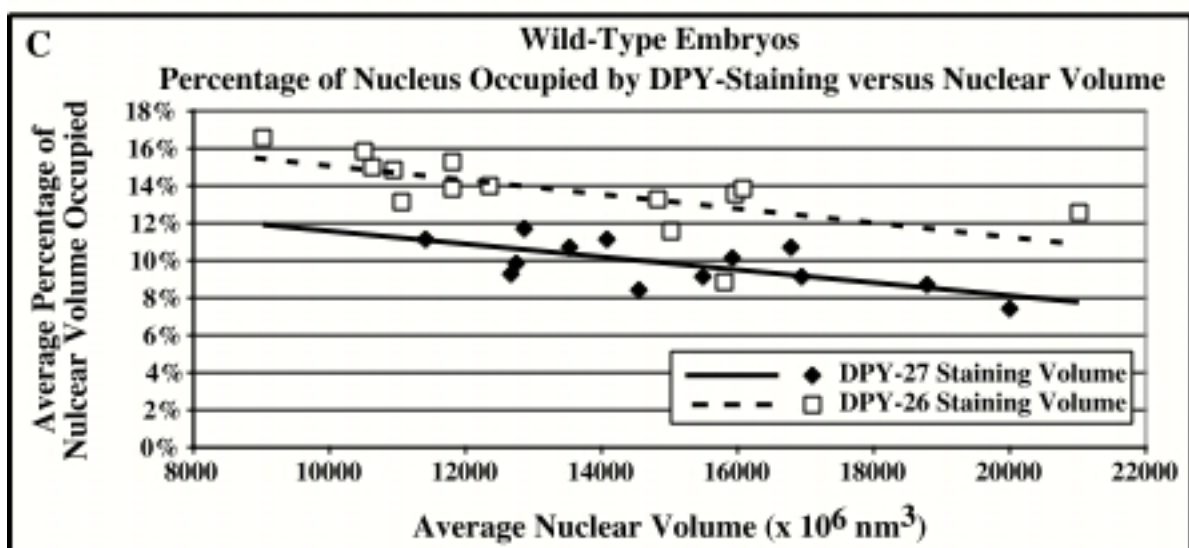
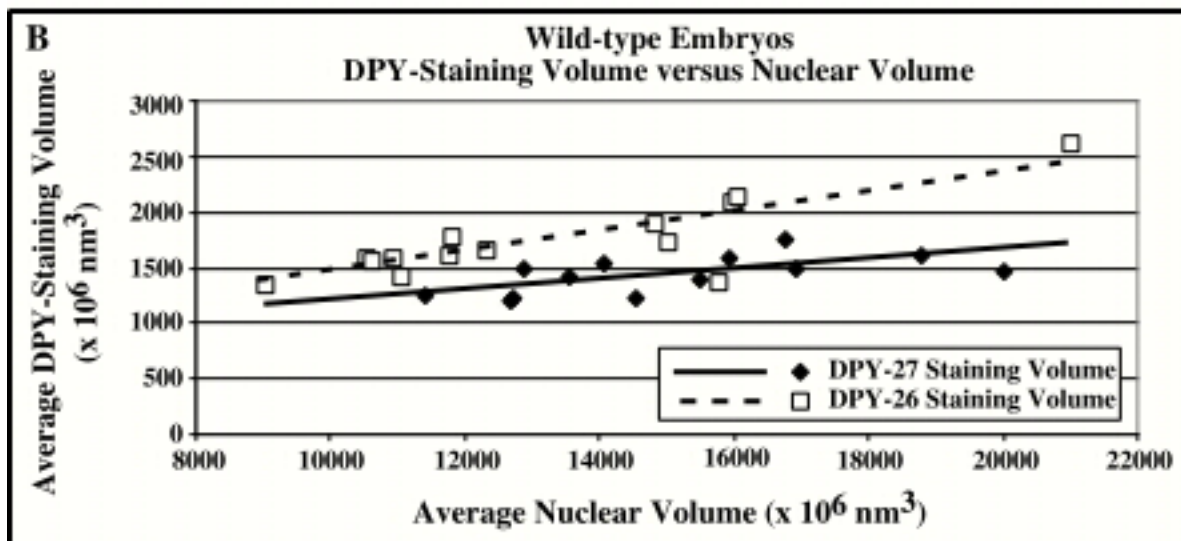
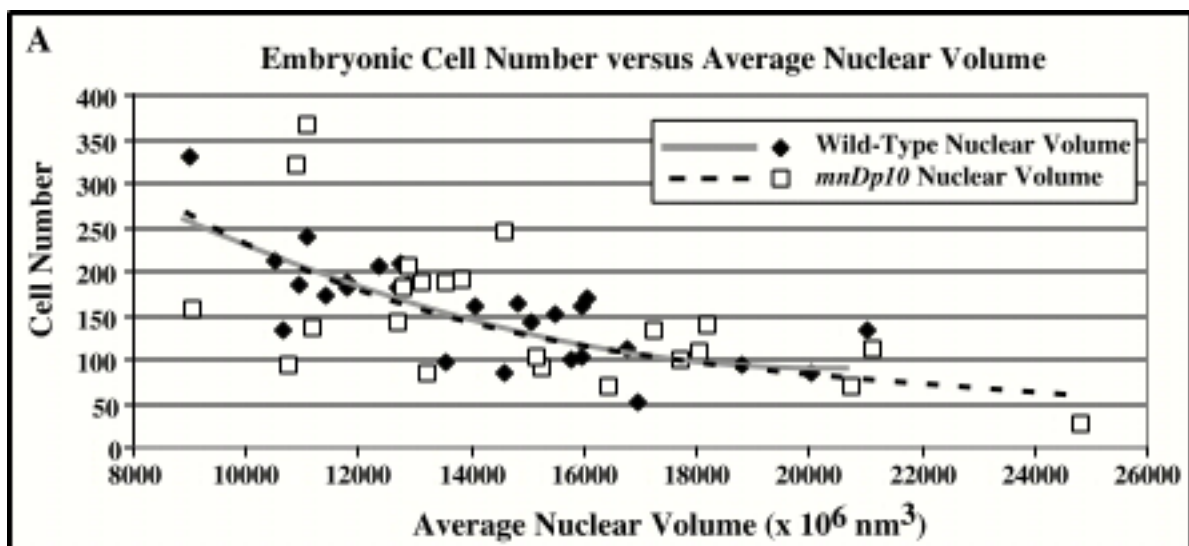


Figure 5.

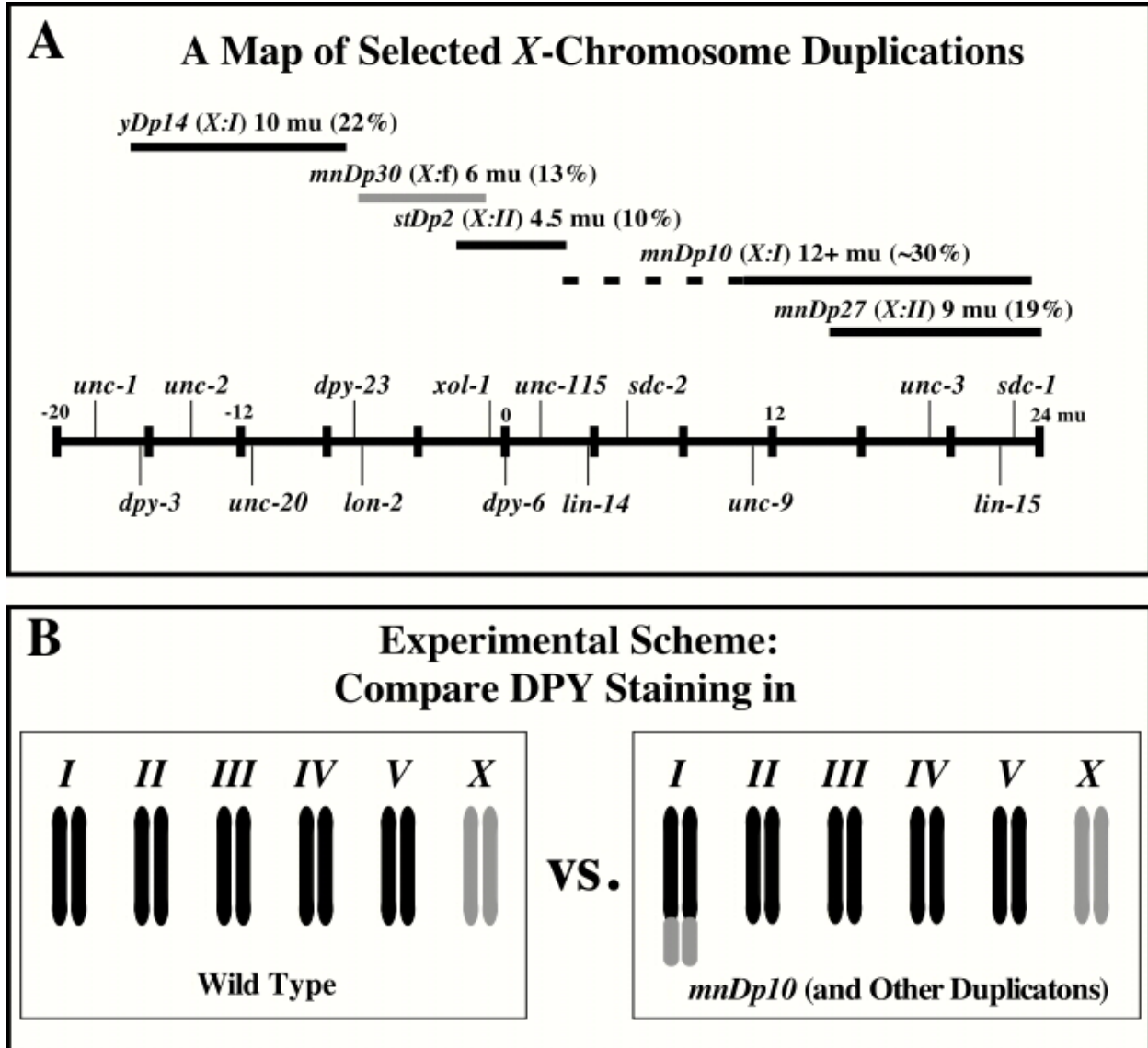


Figure 6.

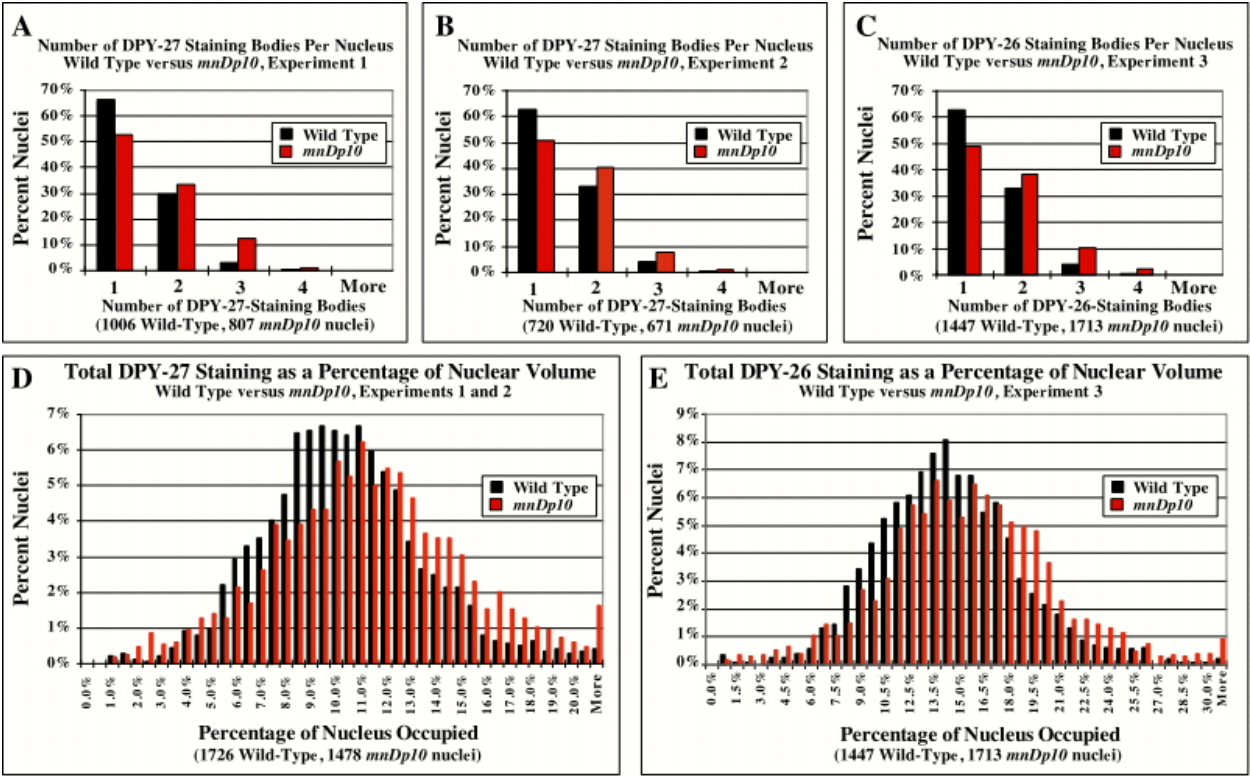


Figure 7.

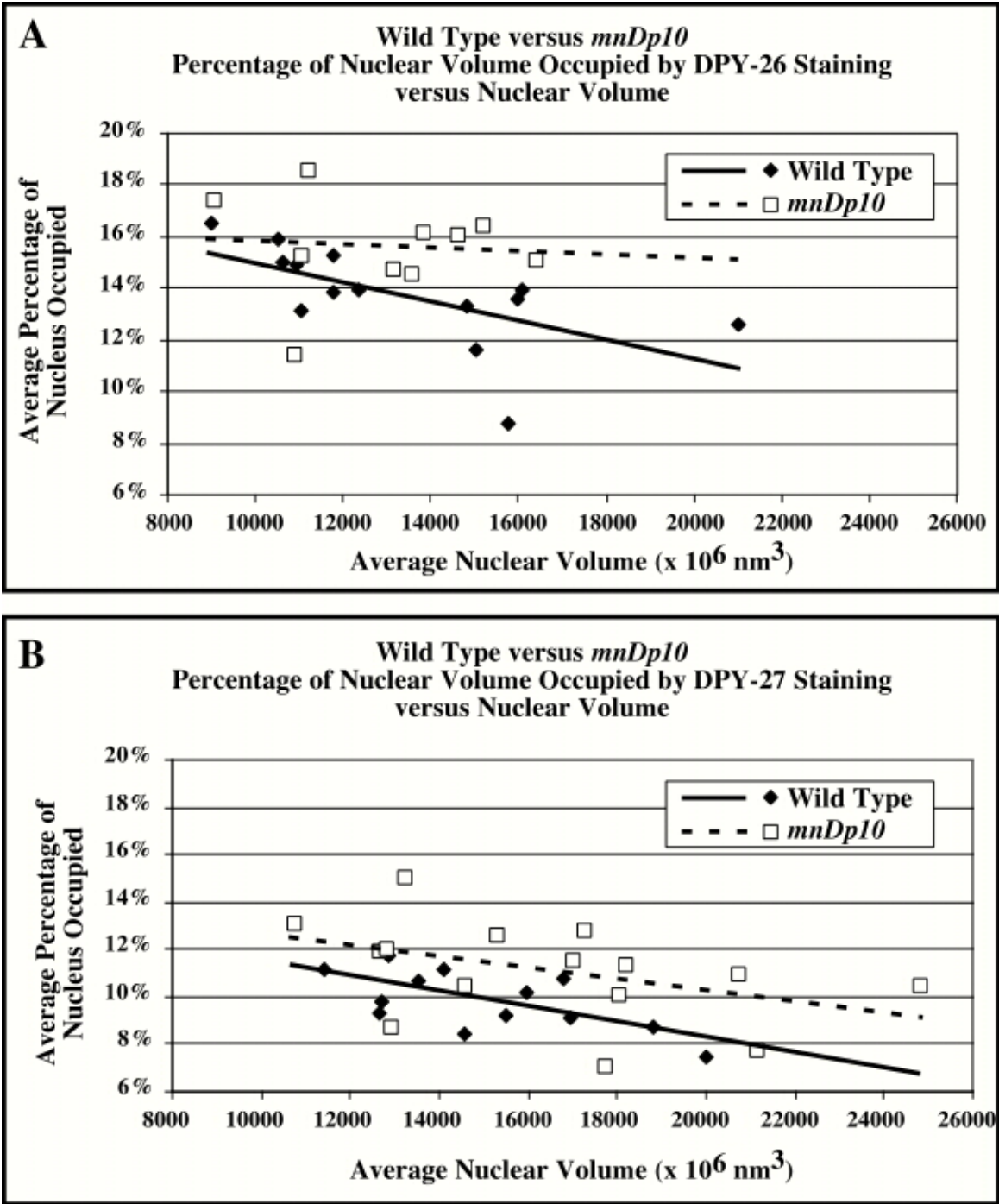


Figure 8.

